Phosphate Adsorption from Wastewater Using Nanostructured Magnetic Core/Shell Adsorbent of $Fe_3O_4/Mn_{0.75}Zn_{0.25}Fe_2O_4$

Akhlaghian, Faranak *+, Mirzapour, Masome

Department of Chemical Engineering, Faculty of Engineering, University of Kurdistan, Sanandaj, I.R. IRAN

ABSTRACT: *Core/shell magnetic nanoparticles of $Fe_3O_4/Mn_{0.75}Zn_{0.25}Fe_2O_4$ were synthesized using the co-precipitation method; and characterized by inductively coupled plasma spectroscopy, Fourier-transform infrared spectroscopy, surface area and porosity analyzer, and transmission electron microscopy techniques. $Fe_3O_4/Mn_{0.75}Zn_{0.25}Fe_2O_4$ nanoparticles were used as an adsorbent to remove phosphate from water. The response surface methodology, central composite design, and Design Expert software version 10 were applied to model the process. The model was used to study the effects of the operating conditions such as pH, adsorbent dose, and phosphate initial concentration. The significance of the model was confirmed by a large F-value, and low p-value. The results indicated that the adsorbent dose had the largest effect on the response. The phosphate adsorption decreased with increasing pH. The adsorption isotherm followed the Langmuir model. The thermodynamic studies showed the endothermic nature of the process. The kinetics of the adsorption was studied, and the experimental data were better fitted to the pseudo-second-order model.*

KEYWORDS: *Phosphate adsorption; Core/shell; Magnetic nanoparticle; Experimental design; Adsorption isotherm.*

INTRODUCTION

Phosphate is used in the production of food, steel, detergents, fertilizers, and pesticides [1-3]. Phosphate is an essential nutrient for all living beings [4]. Excessive amounts of phosphate in water can cause eutrophication. Eutrophication is the excess growth of algae and plants which can decrease dissolved oxygen in water [1-5]. The depletion of dissolved oxygen leads to a decrease in plant photosynthesis [3]. The US Environmental Protection Agency (EPA) has limited phosphate in drinking water to the maximum level of 1 mg/L [1].

Several techniques have been applied to the adsorption of phosphate by water such as electrochemistry, membranes, crystallization, biological processes, chemical precipitation, adsorption, and ion exchange [1-5]. Among them adsorption has many advantages such as low cost, increased yield in dilute solutions, easy operation, fast, and no need to post-treatment stages [1-5].

Adsorption is the rectification of the chemical species by transferring them from fluid to the surface of the solid phase [6]. Adsorption is a surface process; so the surface area is a key parameter in adsorbents [3]. Due to their high surface area, nanoparticles can play an important role in water treatment [7]. Nowadays, magnetic nanoparticles which can be separated from water by applying an external

** To whom correspondence should be addressed.*
+ E-mail: akhlaghianfk@gmail.com
1021-9986/2021/1/157-166 10/$/6.00

magnetic field have attracted considerable attentions. Hydrous lanthanum oxide was loaded on the core/shell magnetic nanoparticles of Fe_3O_4/SiO_2, and was used for the adsorption of phosphate from water by *Lai et al.* They found that adsorbent could be recovered and recycled [8]. *Li et al.* synthesized hollow magnetic nanoparticles of Fe_3O_4/NH_2-MIL101(Fe). They optimized the operating conditions, such as time, adsorbent dose, and pH for phosphate adsorption [2]. The pyridinium-functionalized magnetic nanoparticles of Fe_3O_4/SiO_2 were synthesized by Ma and his coworkers. They used the prepared nanoparticles for phosphate adsorption and studied the effects of time, temperature, pH, and initial concentration on adsorption. They demonstrated that the adsorbent could be regenerated [9].

In this study, core/shell magnetic nanocomposite particles of $Fe_3O_4/Mn_{0.75}Zn_{0.25}Fe_2O_4$ were synthesized by the co-precipitation method and used for the adsorption of phosphate from water. The Response Surface Methodology (RSM), and Central Composite Design (CCD) were used for the experimental design. The optimization of the operating conditions such as initial concentration and pH of the phosphate solution; and adsorbent dose was done using Design Expert software (Version 10). The nature, thermodynamics, and kinetics of the phosphate adsorption were also studied.

EXPERIMENTAL SECTION

Materials

Acetone, ammonium hydroxide, ferric nitrate nonahydrate, ferrous sulfate heptahydrate, hydrazine hydrate, manganese (II) chloride tetrahydrate, potassium dihydrogen phosphate, sodium citrate dihydrate, sodium hydroxide, zinc sulfate heptahydrate, all from Merck Company, were used.

Preparation of the adsorbent

The Fe^{3+} (0.5 M) and Fe^{2+} (0.5 M) solutions were prepared and mixed so that the volumetric ratio of Fe^{3+}:Fe^{2+} was 1.75:1 under protection of nitrogen. 5 mL of hydrazine hydrate and 10 mL of aqueous solution of ammonia were added to the mixture. The addition of ammonia was continued dropwise until the pH of the solution reached 9. Then, the mixture was agitated for 30 min under protection of nitrogen (industrial grade). The black precipitate was collected by an external magnetic field and washed with deionized water until pH reached 7.0. The precipitate was dried at 70°C for 12 h [10, 11].

The citrate ions were loaded on the surface of Fe_3O_4 nanoparticles. The Fe_3O_4 powder (1 g) was dispersed in 200 mL of sodium citrate solution (0.8 M) by an ultrasonic bath. The mixture was stirred under protection of nitrogen at 60°C for 30 min. The precipitate was separated by a magnet and washed with acetone to remove the remainder of the sodium citrate. The precipitate was dried at 70°C in an oven for 12 h [10, 11].

In a flask; 50 mL of $MnCl_2$ (0.49 mol/L), $ZnSO_4$ (0.6 mol/L), and $Fe(NO_3)_3$ (1.91 mol/L); and 2.17 g of Fe_3O_4 modified by citrate were mixed under protection of nitrogen at 90°C for 10 min. 50 mL of NaOH (0.25 mol/L) was added and mixed for 2 h. The precipitate was collected by a magnet and washed with deionized water until the pH of the washing water reached 7.0 [10, 11].

Characterization of the adsorbent

The elemental analysis of the shell and core/shell nanoparticles was performed by the inductively coupled plasma (ICP-OES, Varian). The Fourier transform infrared spectrometer (Vector 22, Bruker) was applied to recognize and compare the chemical bonds and functional groups. Philips CM30 transmission electron microscope (TEM) was used to study the structure of the nanoparticles. The porosity and surface area of the adsorbent were determined by N_2 adsorption/desorption techniques (ASAP 2020 Micrometrics).

Phosphate adsorption

For phosphate adsorption, core/shell magnetic nanoparticles of $Fe_3O_4/Mn_{0.75}Zn_{0.25}Fe_2O_4$ were added to 50 mL of phosphate solution. The mixture was stirred for 3 h. After adsorption, the adsorbent was separated by a magnet. The concentration of phosphate was determined by ammonium molybdate spectrometric method [2]. The phosphate removal (%) was calculated by Equation (1) [2, 12]:

$$\text{Phosphate removal}(\%) = \frac{C_i - C_f}{C_i} \times 100 \quad (1)$$

where C_i, and C_f (mg/L) represent initial and final concentration of the solution, respectively.

The response surface methodology, and central composite design were used to study the effects of the operating conditions such as initial concentration, and pH of the phosphate solution; and adsorbent dose.

Table 1: Experimental design and responses.

Run	Independent Variables			Response, Phosphate removal (%)	
	pH	Phosphate concentration (mg/L)	Adsorbent dose (g/50 mL)	Experimental	Modeling
1	4	162.5	0.81	53.4	55.55
2	6	125	0.63	15.00	15.45
3	6	125	0.25	10.89	9.34
4	6	125	0.63	15.00	15.45
5	8	87.5	0.81	54.00	52.73
6	6	50	0.63	82.26	79.69
7	8	87.5	0.44	34.89	37.98
8	8	162.5	0.44	1.53	3.89
9	8	162.5	0.81	16.86	18.63
10	6	125	0.63	15.00	15.45
11	4	87.5	0.81	86.00	88.06
12	6	125	0.63	15.00	15.45
13	6	125	1.00	68.00	67.05
14	2	125	0.63	86.00	82.43
15	4	162.5	0.44	10.64	13.35
16	6	125	0.63	19.32	15.45
17	4	87.5	0.44	46.82	45.89
18	6	125	0.63	15.00	15.45

Table 1 shows the experimental design and responses. The independent variables were the operating conditions parameters including initial concentration and pH of the solution, and adsorbent dose. The response was the phosphate removal (%).

RESULTS AND DISCUSSION

Characterization

The metal analyses of the samples were done by ICP. The composition of the shell was Mn 25%, Fe 65.34%, and Zn 9.66%. The composition of the core/shell nanoparticles was Mn 12.56%, Fe 82.59%, and Zn 4.85%. Therefore, the formulation of core/shell nanoparticles was determined as follows: $Fe_3O_4/Mn_{0.75}Zn_{0.25}Fe_2O_4$.

The FTIR spectra of Fe_3O_4, modified Fe_3O_4 by citrate, and core/shell nanoparticles of $Fe_3O_4/Mn_{0.75}Zn_{0.25}Fe_2O_4$ are shown in Fig. 1. In the FTIR spectrum of Fe_3O_4, peaks at 1647, and 3182 cm^{-1} are related to the starching and bending hydroxyl bound of the adsorbed water on the surface of Fe_3O_4. The peak at 1386 cm^{-1} is related to the stretching vibration bound of C-O of the adsorbed carbon dioxide. The stretching vibrations of the Fe-O bound are appeared at 462 and 617 cm^{-1} [13-15]. The FTIR spectrum

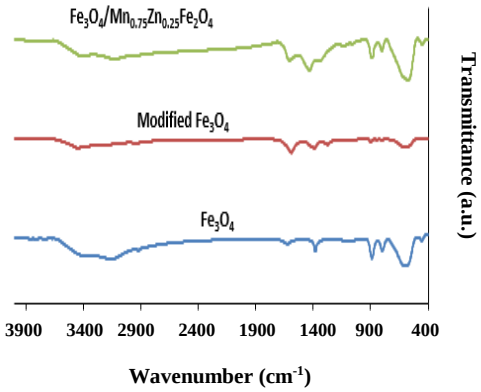

Fig. 1: FTIR spectra of Fe_3O_4, Fe_3O_4 modified by citrate, and $Fe_3O_4/Mn_{0.75}Zn_{0.25}Fe_2O_4$ nanoparticles.

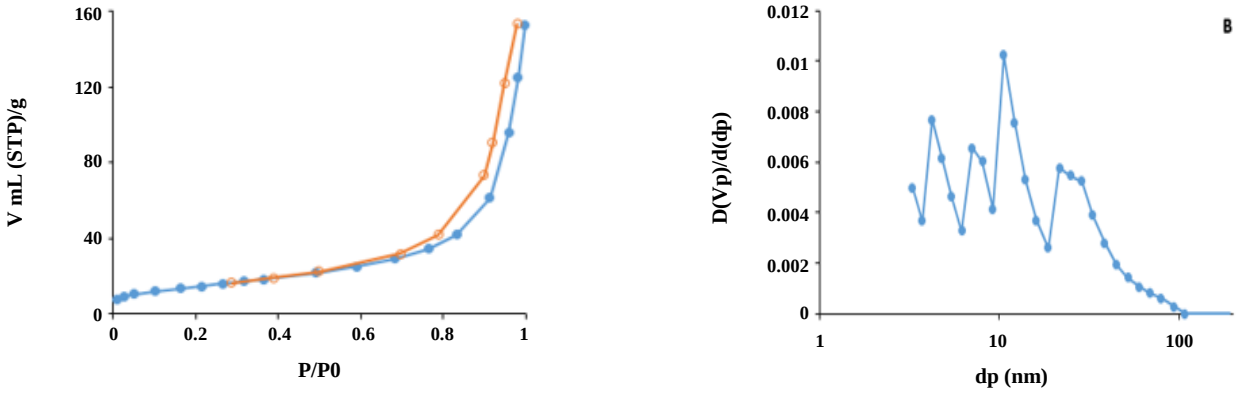

Fig. 2: (A) Nitrogen adsorption/desorption isotherm for $Fe_3O_4/Mn_{0.75}Zn_{0.25}Fe_2O_4$; (B) Pore size distribution according to the BJH desorption isotherm.

of the modified Fe_3O_4 by citrate reveals a peak at 595 cm^{-1} which is related to the stretching vibration of the Fe-O bound. The peak at 1591 cm^{-1} is attributed to the carboxylate bounds confirming that citrate with carboxylate anions are loaded on the surface of Fe_3O_4 [10, 14]. The FT-IR pattern of the core/shell $Fe_3O_4/Mn_{0.75}Zn_{0.25}Fe_2O_4$ shows peaks at 595, and 811 cm^{-1} which confirm the existence of metal-oxygen bound in the structure of the core/shell nanoparticles [10, 16].

Fig. 2(A) shows the nitrogen adsorption/desorption isotherm for $Fe_3O_4/Mn_{0.75}Zn_{0.25}Fe_2O_4$. The adsorbent was macroporous type II. Adsorption is single layer at low pressure, but multilayer adsorption can occur at high pressure. The hysteresis type was H3 which means that the adsorbate formed agglomerated particles with nonuniform slit-shaped pores. Fig. 2(B) shows the pore-size distribution using BJH desorption isotherm. Distribution of the pore size was multimodal. The prevalence of the pores decreased as pore sizes increased [17]. The specific surface area, total pore volume, and mean pore diameter were: 57.65 m^2/g, 0.24 m^3/g, and 10.55 nm; respectively according to the BJH desorption isotherm. The core/shell structure of the nanoparticles are observed in the TEM image of Fig. 3.

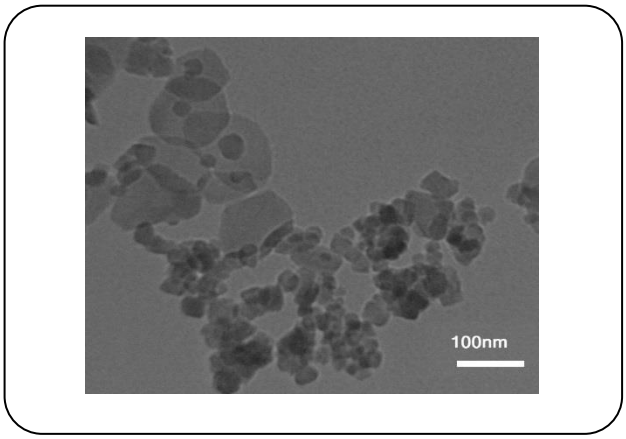

Fig. 3: TEM image of the $Fe_3O_4/Mn_{0.75}Zn_{0.25}Fe_2O_4$.

Experimental design

The batch experiments of the phosphate adsorption were carried out according to Table 1. In each experiment, 50 mL of phosphate solution was used for 3 h. Table 1 shows the phosphate removals (%). All the experiments were replicated three times, and their average was reported.

From the modeling of the results, the third order equation was obtained as follows:

$$\text{Phosphate removal}(\%) = 234.27063 - 26.88991 \times A - 1.81897 \times B - 17.37663 \times C - 18.55312 \times A \times C + 2.77037 \times A^2 + (5.62626E-3) \times B^2 + 164.51717 \times C^2 - (2.1090E-5) \times A \times B^2 \quad (2)$$

Where *A* is the *pH*, *B* is the initial concentration of the phosphate solution (mg/L), and *C* is the adsorbent dose (g/50 mL). Table 2 shows the results of the variance analysis. F-value showed that the differences between standard deviations of the two populations. F-value is the variances ratio of the two populations. Here, two populations are the experimental and modeling results. p-value is the probability that the results happened by chance [18]. The model high F-value (443.6), and low p-value

Table 2: Analysis of Variance.

	Sum of squares	df	Mean square	F-value	p-value prob>F	
Model	14102.50	8	1762.81	443.6	<0.0001	Significant
A (pH)	305.79	1	305.79	76.96	<0.0001	
B (Phosphate concentration, mg/L)	2187.57	1	2187.57	550.56	<0.0001	
C (Adsorbent dose, g/50 mL)	3200.68	1	3200.68	805.56	<0.0001	
AC	294.28	1	294.28	74.11	<0.0001	
A^2	212.35	1	212.35	53.44	<0.0001	
B^2	784.86	1	784.86	197.53	<0.0001	
C^2	878.49	1	878.49	221.10	<0.0001	
AB^2	65.04	1	65.04	16.37	0.0029	
Residues	65.04	1	65.04			
Lack of Fit	20.21	4	5.05	1.62	0.3009	Not Significant
Pure Error	15.55	5	3.11			
Cor Total	14138.26	17				

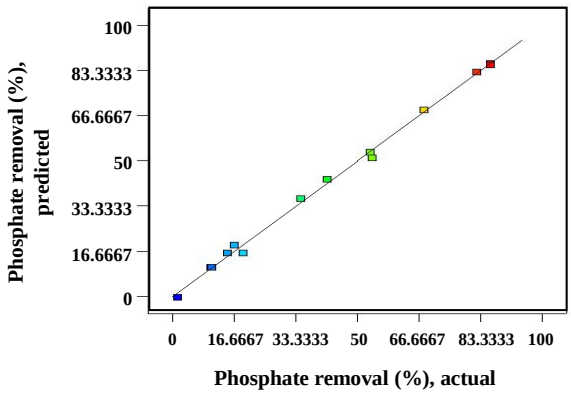

Fig. 4: Predicted results versus experimental for phosphate removal (%).

(<0.0001) showed that the model was statistically significance at the 99.99% confidence level.

As Table 2 shows, linear term of adsorbent dose (C) with the F-value of 805.53 imposed the greatest effect on the phosphate removal (%), and after that the linear term of phosphate concentration (B) with the F-value of 550.56 had more effects on the phosphate adsorption. The interaction term between pH and adsorbent dose (AC) with the F-value of 74.11and interaction term between pH and phosphate concentration (AB^2) with the F-value of 16.37 had the lowest effects on the response. Fig. 4 shows the predicted values versus experimental ones. From Fig. 4 and the values of R^2 (0.9975), and Adj R^2 (0.9952), it can be concluded that there was a good fitness between experimental and modeling results.

Effects of the operating conditions

Fig. 5 shows the effects of the operating conditions. As Fig. 5(A) shows, phosphate adsorption decreased with increasing pH. At low pH, the adsorbent surface would be protonated and positively charged. The attractive electrostatic force between positively charged adsorbent and negatively ions ($H_2PO_4^-$, and HPO_4^{2-}) increased adsorption. At high pH, the repulsive electrostatic force between negatively charged adsorbent, and phosphate ions, as well as competition between hydroxyl and phosphate anions decreased phosphate adsorption [12].

As Fig. 5(B) shows, phosphate adsorption decreased with the increase in phosphate concentration due to the decrease in the ratio of available surface or active site for adsorption to the phosphate concentration. When adsorbent dose increased, phosphate adsorption increased (Fig. 5(C)). Phosphate adsorption increased because of the increase in the adsorption surface area and active sites [12, 19, 20].

Optimization of the operating conditions

The goal of the optimization is to maximize the phosphate removal (%). The Design Expert software (Ver. 10) was used for the optimization. The optimum point

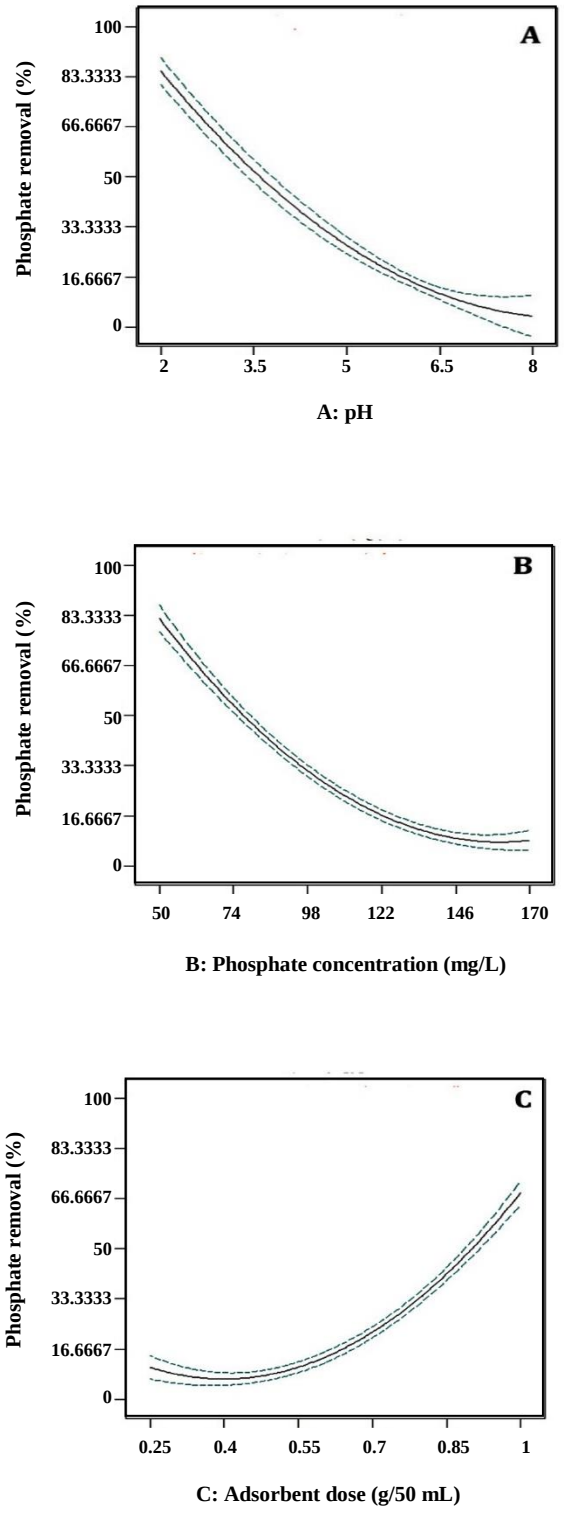

Fig. 5: Effects of (A) pH; (B) Initial concentration of phosphate solution; (C)Adsorbent dose; operating conditions were pH 6, phosphate initial concentration 125 mg/L, adsorbent dose 0.63 g/50 mL, time 3 h; expect the effect of it was investigated.

was selected from the points recommended by Design Expert software (Ver. 10). Table 3 shows the results of the comparison between modeling and experiment for the selected point.

Adsorption isotherm

The adsorption isotherms help to study the interaction of the adsorbent-adsorbate. Langmuir, Freundlich, Dobbin-Radushkevich, and Temkin isotherms were used to study the phosphate adsorption. Table 4 presents the linear form of these models and their parameters [21, 22]. Fig. 6 shows the experimental data versus the linear model. The Langmuir model had the best agreement with the experimental data due to the largest R^2. The Langmuir maximum adsorption capacity was 30.77 mg/g. After the Langmuir model, the Freundlich model had the best fitness to the experimental data.

Thermodynamic of the adsorption

The thermodynamic parameters of the phosphate adsorption of $Fe_3O_4/Mn_{0.75}Zn_{0.25}Fe_2O_4$ including enthalpy (ΔH), entropy (ΔS), and Gibbs free energy are calculated by the following Equations [23, 24]:

$$K = m\frac{q_e}{C_e} \tag{3}$$

$$q_e = \frac{(C_0 - C_e)v}{m} \tag{4}$$

$$Ln\,K = \frac{\Delta S^\circ}{R} - \frac{\Delta H^\circ}{RT} \tag{5}$$

$$\Delta G^\circ = \Delta H^\circ - T\Delta S^\circ \tag{6}$$

Where K is the equilibrium concentration, q_e is the equilibrium adsorption capacity (mg/g), C_e is the equilibrium concentration of the phosphate solution (mg/L), m is the adsorbent dose (g/L), v is the volume of the phosphate solution (L). Fig. 7 shows the values of the enthalpy (ΔH°) and (ΔS°) determined from the slope and intercept of the line of Ln K versus 1/T (Van't Hoff plot). Table 5 shows the calculated thermodynamic parameters. In the temperature range of 298-333 K, the phosphate adsorption process was endothermic because of the positive enthalpy. The negative values of the Gibbs free energies (ΔG°) showed the spontaneous nature of the adsorption process.

Table 3: Operating conditions of the selected optimum point.

Operating conditions			Phosphate removal (%)	
pH	Phosphate concentration (mg/L)	Adsorbent dose (g/50 mL)	Experimental	Modeling
4	87.5	0.81	85.00	88.06

Table 4: Adsorption isotherms model and their parameters [21, 22].

Model	Linear equation	Parameters	
Langmuir	$\frac{C_e}{q_e} = \frac{1}{K_L q_m} + \frac{C_e}{q_m}$	q_m (mg/g)	30.77
		K_L (L/mg)	0.7
		R^2	0.9845
Freundlich	$\mathrm{Log}\, q_e = \mathrm{Log}K_f + \left(\frac{1}{n}\right)\mathrm{Log}C_e$	n	4.79
		K_F	14.6
		R^2	0.842
Dubbin-Radushkevich	$\mathrm{Ln}q_e = \mathrm{Ln}q_m - \beta\varepsilon^2$	q_m (mg/g)	30.89
	$\varepsilon = RT\left(1 + \frac{1}{C_e}\right)$	β (mol^2/kJ^2)	8.1911
	$E = (2\beta)^{-\frac{1}{2}}$	E (kJ/mol)	0.247
		R^2	0.6705
Temkin	$q_e = \beta\mathrm{Ln}K_t + \beta\mathrm{Ln}C_e$	β (kJ/mol)	6.0211
		k_t (L/mg)	4.63
		R^2	0.8292

Kinetics of the adsorption

Phosphate adsorption on $Fe_3O_4/Mn_{0.75}Zn_{0.25}Fe_2O_4$ nanoparticles is affected by the contact time that phosphate ions presented in the interface of solid-liquid and diffusion path. The kinetic studies are important to predict the adsorption rate, and also provide valuable information to find out the mechanism of the adsorption process [6].

The two most famous kinetic models are pseudo first order model and pseudo second order model [23, 24]. Table 6 presents the linear forms of these models with their parameters. Fig. 8 shows the results of the fitting experimental data to the linear models. The calculated parameters are shown in Table 6. The experimental data followed the pseudo second order model due to its larger R^2. Therefore, chemisorption of the phosphate on the $Fe_3O_4/Mn_{0.75}Zn_{0.25}Fe_2O_4$ is the rate controlling step in the adsorption [23, 24].

CONCLUSIONS

Excess amount of phosphate in water causes eutrophication phenomenon and decrease the quality of water. Therefore, it is necessary to remove phosphate from water. In this work, a novel magnetic core/shell adsorbent was used for phosphate removal. Co-precipitation method was used to synthesize the core/shell nanoparticles. The chemical formula of the nanoparticles was determined by ICP: $Fe_3O_4/Mn_{0.75}Zn_{0.25}Fe_2O_4$. The results of characterization by FTIR showed the formation of the oxygen-metal bond. The TEM image showed the core/shell structure of $Fe_3O_4/Mn_{0.75}Zn_{0.25}Fe_2O_4$. The porosimetry revealed the macro porous structure of the type II and hysteresis type H3. The $Fe_3O_4/Mn_{0.75}Zn_{0.25}Fe_2O_4$ nanoparticles were used as adsorbent to remove of phosphate from water. The effects of the operating conditions such as adsorbent dose, pH,

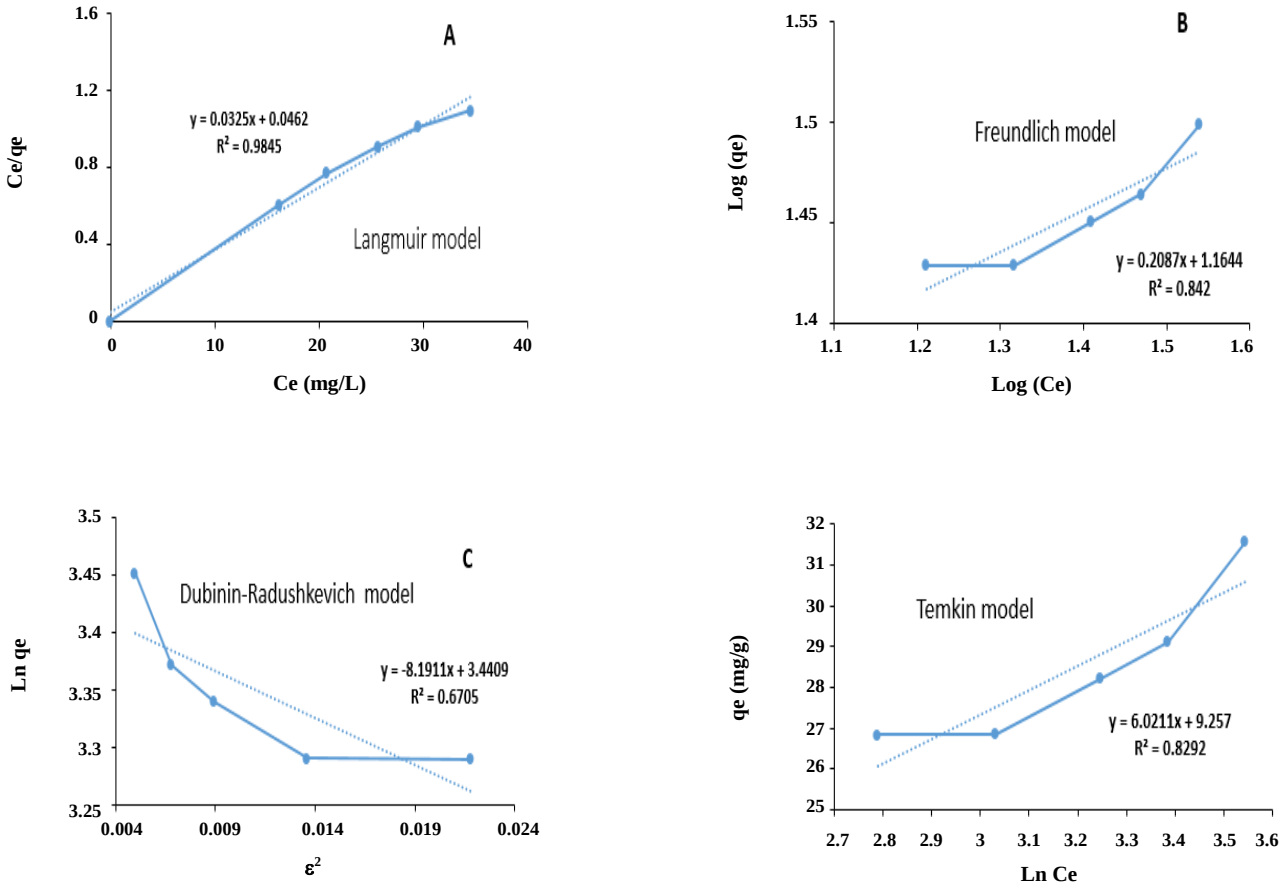

Fig. 6: The adsorption isotherms; (A) Langmuir; (B) Freundlich; (C) Dobbin-Radushkevich; (D) Temkin

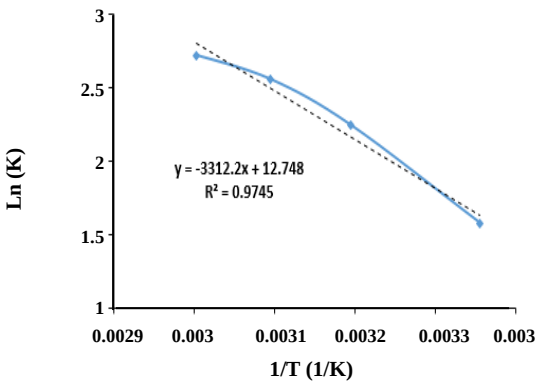

Fig. 7: Van't Hoff plot for the adsorption of phosphate on $Fe_3O_4/Mn_{0.75}Zn_{0.25}Fe_2O_4$.

and initial concentration of phosphate in water were investigated. Design Expert software (Ver. 10) was used to model and optimize the operating conditions. Central composite design method was used for experimental design. There was a good agreement between experimental and software modeling results. The results showed that adsorbent dose had the highest effect on the phosphate adsorption. The Langmuir, Freundlich, Dobbin-Radushkevich, and Temkin isotherms were applied to study the phosphate adsorption. The Langmuir isotherm had the best fitness to the experimental data. The Langmuir maximum adsorption capacity was 30.77 mg/g. The thermodynamic analysis showed positive enthalpy and endothermic process. The kinetic studies indicated that pseudo second order model was the best to show the behavior of the adsorption. The high adsorption capacity for phosphate removal and the magnetic property of the adsorbent which makes its separation from water easy show the promising future of this adsorbent.

Table 5: Thermodynamic parameters of the phosphate adsorption on $Fe_3O_4/Mn_{0.75}Zn_{0.25}Fe_2O_4$.

Phosphate initial concentration (mg/L)	ΔH° (J/mol)	ΔS (J/mol.K)	-ΔG (J/mol)			
			298 K	313 K	323 K	333 K
80	53527.97	105.9203	2908.37	5839.78	6868.24	7534.36

Table 6: Kinetic models and their parameters for phosphate adsorption.

Model	Linear equation	Parameters	
Pseudo first order	$Ln(q_e - q_t) = Lnq_e - k_1 t$	q_e (mg/g)	13.13
		k_1 (min^{-1})	0.007
		R^2	0.9209
Pseudo second order	$\frac{t}{q_t} = \frac{1}{k_2 q_e^2} + \frac{t}{q_e}$	q_e (mg/g)	18.52
		k_2 (g mg^{-1} min^{-1})	0.1
		R^2	0.9987

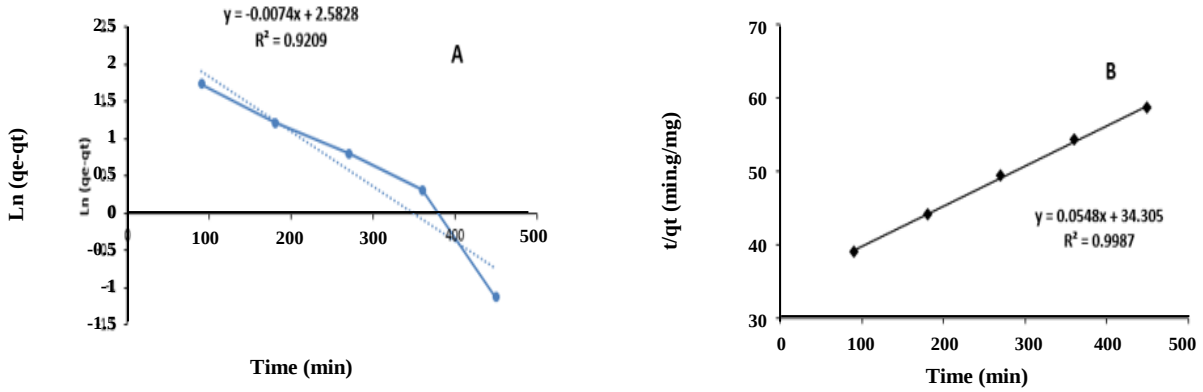

Fig. 7: Van't Hoff plot for the adsorption of phosphate on $Fe_3O_4/Mn_{0.75}Zn_{0.25}Fe_2O_4$.

Acknowledgments

The authors gratefully acknowledge the financial support of the University of Kurdistan.

Received : Jun. 22, 2019 ; Accepted : Oct. 10, 2019

REFERENCES

[1] Mehrabi N., Soleimani M., Sharififard H., Madadi Yeganeh M., Optimization of Phosphate Removal from Drinking Water with Activated Carbon Using Response Surface Methodology (RSM), *Desalin. Water Treat.*, **57(133)**: 1-6 (2015).

[2] Li Y., Xie, Q., Hu Q., Li C., Huang Z., Yang X., Guo H., Surface Modification of Hollow Magnetic Fe_3O_4@NH_2- MIL-101(Fe) Derived from Metal-Organic Frameworks for Enhanced Selective Removal of Phosphates from Aqueous Solution, *SCi. Rep.-UK*, **6**: 30651-30662 (2016).

[3] Arshadi M., Etemad Gholtash J., Zandi H., Foroughifard S., Phosphate Removal by a Nano-Biosorbent from the Synthetic and Real (Persian Gulf) Water Samples, *RSC Adv.*, **5**: 43290-43302 (2015).

[4] Li G., Gao S., Zhang G., Zhang X., Enhanced Adsorption of Phosphate from Aqueous Solution by Nanostructured Iron(III)-Copper(II) Binary Oxides, *Chem. Eng. J.*, **235**: 124-131 (2014).

[5] Rodrigues L.A, Caetano M.L., da Silva P., Adsorption Kinetic, Thermodynamic and Desorption Studies of Phosphate onto Hydrous Niobium Oxide Prepared by Reverse Microemulsion Method, Adsorption, **16**: 173-181 (2010).

[6] Worch E., "Adsorption Technology in Water Treatment", Walter de Gruyter GmbH & Co. KG, Berlin/Boston (2012).

[7] Shah N., Claessyns F., Rimmer S., Arain M.B., Rehan T., Wazwaz A., Ahmad M.W., Ul-Islam M., Effective Role of Magnetic Core-Shell Nanocomposites in Removing Organic and Inorganic Wastes from Water, *Recent Pat. Nanotech.*, **10**: 202-212 (2016).

[8] Lai L., Xie Q., Chi L., Gu W., Wu D., Adsorption of Phosphate from Water by Easily Separable Fe_3O_4@SiO_2 Core/Shell Magnetic Nanoparticles Functionalized With Hydrous Lanthanum Oxide, *J. Colloid Interf. Sci.*, **465**: 76-82 (2016).

[9] Ma F., Du H., Li R., Zhang Z., Pyridinium-Functionalized Magnetic Mesoporous Silica Nanoparticles as a Reusable Adsorbent for Phosphate Removal from Aqueous Solution, *Water Sci. Technol.*, **74(5)**: 1127-1135 (2016).

[10] Hong R.Y., Li J.H., Cao X., Zhang S.Z., Dic G.Q., Li H.Z., Wei D.G., On the $Fe_3O_4/Mn_{1-x}Zn_xFe_2O_4$ Core/Shell Magnetic Nanoparticles, *J. Alloys Comp.*, **480**: 947-953 (2009).

[11] Mirzapour M., Akhlaghian F., Core/shell Magnetic Nanoparticles of $Fe_3O_4/Mn_xZn_yFe_{3-x-y}O_4$ for Phosphate Adsorption from Water: Effects of Adsorbent Composition Using Response Surface Methodology, *Desalin. Water Treat.*, **137**: 114-127 (2019).

[12] Yan L., Yang K., Shan R., Yan T., Wei J., Yu S., Yu H., Du B., Kinetic, Isotherm and Thermodynamic Investigations of Phosphate Adsorption onto Core-Shell Fe_3O_4@LDHs Composites with Easy Magnetic Separation Assistance, *J. Colloid Interf. Sci.*, **448**: 508-516 (2015).

[13] Ghosh A., Pal M., Biswas K., Ghosh U.C., Manna B., Manganese Oxide Incorporated Ferric Oxide Nanocomposites (MIFN): A Novel Adsorbent for Effective Removal of Cr(VI) From Contaminated Water, *J. Water Process. Eng.*, **7**: 176-186 (2015).

[14] Absalan G., Asadi M., Kamran S., Sheikhian L., Goltz D.M., Removal of Reactive Red-120 and 4-(2-Pyridylazo) Resorcinol from Aqueous Samples by Fe_3O_4 Magnetic Nanoparticles Using Ionic Liquid as Modifier, *J. Hazard. Mater.*, **192**: 476-484 (2011).

[15] Hong R.Y., Zhang S.Z., Di G.Q., Li H.Z., Zheng Y., Ding J., Wei D.G., Preparation, Characterization and Application of Fe_3O_4/ZnO Core/shell Magnetic Nanoparticles, *Mater. Res. Bull.*, **43**: 2457-2468 (2008).

[16] Parikh S.J, Chorover J., FT-IR Spectroscopic Study of Biogenic Mn-Oxide Formation by *Pseudomonas putida* GB-1, *Geomicrobiol. J.*, **22**: 207-218 (2005).

[17] Leofanti G., Padovan M., Tozzola G., Venturelli B., Surface Area and Pore Texture of Catalysts, *Catal. Today*, **41**: 207-219 (1998).

[18] Montgomery D.C., "Design and Analysis of Experiments", 5th ed., John Wiley and Sons (2012).

[19] Ballav N., Choi H.J., Mishra S.B., Maity A., Synthesis, Characterization of Fe_3O_4@Glycine Doped Polypyrrole Magnetic Nanocomposites and Their Potential Performance to Remove Toxic Cr(VI), *J. Ind. Eng. Chem.*, **20(6)**: 4085-4093 (2014).

[20] Nameni M., Alavi Moghadam M.R., Arami M., Adsorption of Hexavalent Chromium from Aqueous Solutions by Wheat Bran, *Int. J. Environ. Sci. Tech.*, **5(2)**: 161-168 (2008).

[21] Mehrabi N., Soleimani M., Madadi Yeganeh M., Sharififard H., Parameters Optimization for Nitrate Removal from Water Using Activated Carbon and Composite of Activated Carbon and Fe_2O_3 Nanoparticles, *RSC Adv.*, **5**: 51470-51482 (2015).

[22] Dada A.O, Olalekan A.P, Olatunya A.M., DADA O., Langmuir, Freundlich, Temkin and Dubinin–Radushkevich Isotherms Studies of Equilibrium Sorption of Zn^{2+} onto Phosphoric Acid Modified Rice Husk, *ISOR J. Appl. Chem.*, **3(1)**: 38-45 (2012).

[23] Akhlaghian F., Souri B., Mohamadi Z., Nanostructured Fe_2O_3/Al_2O_3 Adsorbent for Removal of As (V) from Water, *Adv. Environ. Technol.*, **2**: 67-75 (2017).

[24] Tahir H., Saud A., Saad M., Synthesis of Kaolin Loaded Ag and Ni Nanocomposites and Their Applicability for the Removal of Malachite Green Oxalate Dye , *Iran. J. Chem. Chem. Eng. (IJCCE)*, **37(3)**: 11-22 (2018).